11-10-2016

125Te NMR and Seebeck Effect in Bi2Te3 Synthesized from Stoichiometric and Te-Rich Melts

E. M. Levin
Iowa State University and Ames Laboratory

Trevor M. Riedemann
Ames Laboratory, tmr@ameslab.gov

A. Howard
Ames Laboratory

Na Hyun Jo
Iowa State University, njo@iastate.edu

Sergey L. Bud'ko
Iowa State University and Ames Laboratory, budko@ameslab.gov
See next page for additional authors

125Te NMR and Seebeck Effect in Bi2Te3 Synthesized from Stoichiometric and Te-Rich Melts

Abstract

Bi2Te3 is a well-known thermoelectric material and, as a new form of quantum matter, a topological insulator. Variation of local chemical composition in Bi2Te3 results in formation of several types of atomic defects, including Bi and Te vacancies and Bi and Te antisite defects; these defects can strongly affect material functionality via generation of free electrons and/or holes. Nonuniform distribution of atomic defects produces electronic inhomogeneity, which can be detected by 125Te nuclear magnetic resonance (NMR). Here we report on 125Te NMR and Seebeck effect (heat to electrical energy conversion) for two single crystalline samples: (#1) grown from stoichiometric composition by Bridgman technique and (#2) grown out of Te-rich, high temperature flux. The Seebeck coefficients of these samples show p- and n-type conductivity, respectively, arising from different atomic defects. 125Te NMR spectra and spin–lattice relaxation measurements demonstrate that both Bi2Te3 samples are electronically inhomogeneous at the atomic scale, which can be attributed to a different Te environment due to spatial variation of the Bi/Te ratio and formation of atomic defects. Correlations between 125Te NMR spectra, spin–lattice relaxation times, the Seebeck coefficients, carrier concentrations, and atomic defects are discussed. Our data demonstrate that 125Te NMR is an effective probe to study antisite defects in Bi2Te3.

Disciplines

Biological and Chemical Physics | Materials Chemistry | Materials Science and Engineering | Physical Chemistry

Comments

This document is the Accepted Manuscript version of a Published Work that appeared in final form in *The Journal of Physical Chemistry C*, copyright © American Chemical Society after peer review and technical editing by the publisher. To access the final edited and published work see DOI: 10.1021/acs.jpcc.6b06973. Posted with permission.

Authors

E. M. Levin, Trevor M. Riedemann, A. Howard, Na Hyun Jo, Sergey L. Bud'ko, Paul C. Canfield, and Thomas A. Lograsso

10-11-2016

^{125}Te NMR and Seebeck Effect in Bi_2Te_3 Synthesized from Stoichiometric and Te-rich Melts

E. M. Levin,[1,2*] T. M. Riedemann,[1] A. Howard,[1] N. H. Jo,[2] S. L. Bud'ko,[1,2]
P. C. Canfield,[1,2] and T. A. Lograsso[1,3]

[1] *Division of Materials Sciences and Engineering, U.S. Department of Energy Ames Laboratory, Ames, Iowa 50011, USA*
[2] *Department of Physics and Astronomy, Iowa State University, Ames, Iowa 50011, USA*
[3] *Department of Materials Science and Engineering, Iowa State University, Ames, Iowa 50011, USA*

Submitted to *J. of Physical Chemistry C*

Abstract

Bi_2Te_3 is a well-known thermoelectric material and as a new form of quantum matter, a topological insulator. Variation of local chemical composition in Bi_2Te_3 results in formation of several types of atomic defects, including Bi and Te vacancies, and Bi and Te antisite defects; these defects can strongly affect material functionality via generation of free electrons and/or holes. Non-uniform distribution of atomic defects produces electronic inhomogeneity, which can be detected by ^{125}Te nuclear magnetic resonance (NMR). Here we report on ^{125}Te NMR and Seebeck effect (heat to electrical energy conversion) for two single crystalline samples: (#1) grown from stoichiometric composition by Bridgman technique, and (#2) grown out of Te-rich, high temperature flux. The Seebeck coefficients of these samples show *p*- and *n*-type conductivity, respectively, arising from different atomic defects. ^{125}Te NMR spectra and spin-lattice relaxation measurements demonstrate that both Bi_2Te_3 samples are electronically inhomogeneous at the atomic scale, which can be attributed to a different Te environment due to spatial variation of the Bi/Te ratio and formation of atomic defects. Correlations between ^{125}Te NMR spectra, spin-lattice relaxation times, the Seebeck coefficients, carrier concentrations, and atomic defects are discussed. Our data demonstrates that ^{125}Te NMR is an effective probe to study antisite defects in Bi_2Te_3.

1. INTRODUCTION

Bi_2Te_3 is a narrow band gap semiconductor well-known for its utilization in refrigerating devices due to its large Peltier effect.[1] Bi_2Te_3 has been studied for a long time and various experimental methods have been used to better understand this interesting material. [1-3] Recently, Bi_2Te_3 was considered as a new form of quantum matter, a three-dimensional topological insulator, which stimulates its study as a material for possible spintronic and quantum computing applications.[2,3] The bulk electrical conductivity of Bi_2Te_3 is very sensitive to defects whose occurrence is dependent on the composition and synthesis method. Detailed studies, using several experimental methods, are required to better understand this and related materials.

One of the microscopic techniques used to study complex tellurides, e.g., PbTe- and GeTe-based materials, is nuclear magnetic resonance (NMR). It has been shown that ^{207}Pb[4,5] and ^{125}Te NMR[5-8] spectra and spin-lattice relaxation measurements enable detection of different chemical environments and determination of the carrier concentration. Micro- [9] and nano-size [10] powder Bi_2Te_3 samples were also studied by ^{125}Te NMR. Taylor *et al*.[9] have shown that ^{125}Te NMR spectrum of micro-size powder Bi_2Te_3 ground by mortar and pestle contains one peak at about +400 ppm (parts per 10^6). It was stated that ^{125}Te NMR of micro-size grains reflects properties of bulk Bi_2Te_3.[9] Koumoulis *et al*. [10] have shown that ^{125}Te NMR spectra of nano-scale particles of Bi_2Te_3 prepared by ball-milling contain a main peak at +500 ppm, and in addition, a shoulder at -500 ppm. Unfortunately, the details on the initial bulk samples synthesis and their properties were not reported, but the authors suggest that the size of grains can strongly affect ^{125}Te NMR spectra.

Earlier, we have shown that ^{125}Te NMR enables a better understanding of the chemistry and physics of GeTe- and PbTe-based tellurides related to atomic defects.[5,6,8] It is also well

known that the Bi/Te ratio in Bi_2Te_3 produces a strong effect on electronic properties via formation of various atomic defects,[11] acting even stronger than in GeTe- and PbTe-based materials. Here we report on ^{125}Te NMR spectra and spin-lattice relaxation measurements along with the Seebeck coefficient and Hall effect measurements for two single crystalline Bi_2Te_3 samples, and discuss the effects arising from atomic defects. The samples were prepared by different methods, (i) by Bridgman method from a starting composition of stoichiometric Bi_2Te_3, and (ii) grown out of Te-rich high temperature flux.

2. EXPERIMENTAL DETAILS

Two Bi_2Te_3 samples (#1 and #2) were synthesized using high purity components, 99.999% Bi and 99.999% Te. Bi_2Te_3 (#1) was synthesized by direct melting of constituent components with initial stoichiometry $Bi_{40}Te_{60}$ in a 12 mm diameter fused silica ampoule at 650 ^oC for one hour, stirring periodically. The ingot was then placed in a 15 mm diameter fused silica crucible in argon back-filled up 250 mm Hg pressure atmosphere, sealed, and used for Bridgman single crystal growth at 800 ^oC with the withdrawal rate of 1 mm/hr. Bi_2Te_3 (#2) was grown out of Te-rich melt with initial stoichiometry of $Bi_{25}Te_{75}$ in an alumina crucible. The crucible was sealed in fused silica ampoule [12,13] and heated to 580 ^oC over 3 h, held at 580 ^oC for 3 h, slowly cooled down to 440 ^oC within 60 h, and then decanted using a centrifuge.[12,13] Details about solidification of Bi_2Te_3 from the melts of two initial nominal compositions, $Bi_{40}Te_{60}$ and $Bi_{25}Te_{75}$, can be seen on a Bi-Te phase diagram.[14]

XRD patterns were obtained using a Panalytical X'Pert Pro MPD system with Co-$K\alpha$ radiation (λ = 0.1789 nm) at 300 K; both Bi_2Te_3 samples are found to be single-phase (Figure 1). Bi_2Te_3 crystallizes in the hexagonal structure with three planes, each containing five-atom $Te_{(1)}$-

Bi-$Te_{(2)}$-Bi-$Te_{(1)}$ layers, where Te atoms in the same plane are located in positions $Te_{(1)}$ and $Te_{(2)}$;[15] the structure can be described in terms of hexagonal [16] or rhombohedral structure.[15,17] Lattice parameters of our samples calculated using Rietveld refinements in the program X'Pert HighScore Plus [7] for both hexagonal and rhombohedral structures are shown in Table 1. Note that for Bi_2Te_3 (#2) the main Bragg peak is slightly shifted compared to that for Bi_2Te_3 (#1) (Fig. 1), and calculated lattice parameters are slightly smaller (see Table 1 and discussion below).

^{125}Te nuclear magnetic resonance (NMR) experiments were conducted at 126 MHz using a Bruker 400WB plus spectrometer with TopSpin software in a magnetic field of 9.4 T without sample spinning (static regime). Ten $\pi/2$ pulses with duration of 3 μs were used for saturating the magnetization. Signals were detected after a Hahn echo generated by a 2 μs and 3 μs pulse sequence.[5,7,18] ^{125}Te NMR chemical shifts were referenced to $Te(OH)_6$ in solution and chemical shifts relative to $(CH_3)_2Te$ in benzene were larger by +712 ppm.[18] ^{125}Te NMR spin-lattice relaxation measurements were used to obtain the spin-lattice relaxation time, T_1, and the free (mobile) charge carrier concentration. Saturated recovery time (delay time) was varied from 0.05 to 5000 ms, the number of scans for each delay time was 32k; total measurement time for each sample was about 200 hr. Fitting of the relaxation curves was conducted as described in Ref. 7.

The Seebeck coefficient was measured in the temperature range of 300-700 K using an LSR-3 measuring system (Linseis, Inc.). The time for each measurement was about 4 hours, and measurements were repeated several times in order to check the Seebeck coefficient stability. The measurements uncertainty is ~5%, and no hysteresis in the Seebeck coefficient during temperature cycling was observed. The Hall effect was measured at 300 K using a Quantum Design Physical Properties Measuring System, with the odd in magnetic field data taken as Hall

component. The carrier concentration was estimated from the linear fit magnetic field dependent Hall resistivity in the limit of low magnetic fields.

3. RESULTS AND DISCUSSION

Several different atomic defects are, in general, possible in Bi_2Te_3: (i) vacancies on the Bi sublattice, denoted as V_{Bi}, (ii) vacancies on the Te sublattice, denoted as V_{Te}, (iii) Bi antisite defects (Bi atom substitution of Te atom in the Te sublattice), denoted as Bi_{Te}, (iv) Te antisite defects (Te atom substitution of Bi atom in the Bi sublattice), denoted as Te_{Bi}, and (v) interstitial Bi or Te atoms.[3,19-22] It was shown experimentally by Fleurial *et al*.[11] that depending on the type of defects, which may generate free (mobile) electrons and/or holes, the Seebeck and Hall coefficients can be positive or negative, and different in the magnitude. Atomic defects in Bi_2Te_3 were also studied theoretically and discussed in detail by Scalon *et al*.[3] and by Hashibon and Elsasser. [23]

Figure 2 shows temperature dependencies of the Seebeck coefficient of Bi_2Te_3 (#1) and Bi_2Te_3 (#2). Since the other measurements in this work were performed at 300 K, through the rest of the paper we will refer, in the case of comparison, to the Seebeck coefficient at 300 K. The Seebeck coefficients of Bi_2Te_3 (#1) and Bi_2Te_3 (#2) are +250 $\mu V\ K^{-1}$ and -133 $\mu V\ K^{-1}$, respectively. Any difference found was within the error of measurements for the Seebeck coefficient of both samples between the first and second runs. The sign of the Seebeck coefficient shows that Bi_2Te_3 (#1) is *p*-type (conductivity due to holes), Bi_2Te_3 (#2) is *n*-type (conductivity due to electrons).

Scanlon *et al*.[3] suggested that antisite defects in Bi_2Te_3 in both cases, Bi-rich/Te-poor and Bi-poor/Te-rich, dominate over all other defects including anion and cation vacancies. Tellurium

antisite defects, Te_{Bi}, with the lowest formation energy of all possible defects in Bi_2Te_3 serve as donors and generate electrons with possible compensation by the V_{Bi} defects, which serve as acceptors and generate holes.[3] In our sample Bi_2Te_3 (#2) synthesized from the melt with initial composition of $Bi_{25}Te_{75}$, the contribution from Te_{Bi} defects overcomes those produced by other possible defects.

Bismuth antisite defects, Bi_{Te}, serve as acceptors and generate holes,[3] whereas V_{Te} defects serve as donors. In sample Bi_2Te_3 (#1) synthesized from the melt with initial composition of $Bi_{40}Te_{60}$, the contribution from Bi_{Te} defects overcomes those produced by other possible defects. In both cases, the type of conductivity in Bi_2Te_3 is determined by antisite defects, which agrees well with experimental data by Fleurial *et al*.[11] and theoretical modeling by Scalon *et al*. [3] Both types of antisite defects in our samples are thermally stable, which is demonstrated by similar temperature dependencies of the Seebeck coefficient during the first and following runs (Fig. 2).

Slightly smaller lattice parameters of Te-rich Bi_2Te_3 (#2) compared to that of Bi_2Te_3 (#1) (Table 1) should be attributed to the smaller atomic radii of Te, 0.14 nm, compare to that of Bi, 0.16 nm,[22] which can be present on regular site Te and Bi sites as well as on Te_{Bi} and Bi_{Te} antisites, respectively. This reflects variation in Bi/Te ratio that results from the different growth methods. It is to be expected that there is some width of formation for Bi_2Te_3, especially at high temperatures where growth occurs and solution growth from Te-rich melt will naturally produce a slightly Te enriched composition compared to a stoichiometric growth. This deviation is clearly reflected in all the measurements (see below).

Our Hall effect measurements show the *p*- and *n*-type conductivity of Bi_2Te_3 (#1) and Bi_2Te_3 (#2), and the carrier concentration of 1.2×10^{19} holes/cm^3 and 3.0×10^{19} electrons/cm^3, respectively (Table 2). Within the model for the Seebeck coefficient of metals and degenerate

semiconductors with energy independent scattering, $S \sim 1/n^{2/3}$, where n is the carrier concentration.[24] To compare the Seebeck coefficients and carrier concentrations we can use the relation $S_{\#1} / S_{\#2} = (n_{\#2} / n_{\#1})^{2/3}$. The absolute value of the ratio $S_{\#1} / S_{\#2} = 250\ \mu V\ K^{-1}/133\ \mu V\ K^{-1} = 1.88$ results in $n_{\#2}/n_{\#1} = 2.56$, which agrees well with that obtained from the Hall effect measurements, 2.50, and reflects different concentrations of atomic defects affecting the total charge carrier concentration. Hence, the larger absolute value of the Seebeck coefficient of Bi_2Te_3 (#1) at 300 K compared to that of Bi_2Te_3 (#2) is mostly determined by the lower carrier concentration and can be attributed to lower concentration of antisite defects.

Figure 3 shows ^{125}Te NMR spectra of Bi_2Te_3 (#1) (Fig. 3a) and Bi_2Te_3 (#2) (Fig. 3b). The spectra of both samples exhibit the main peak and the right shoulder. The main peak of ^{125}Te NMR for Bi_2Te_3 (#1) is observed at -270 ppm; a small shoulder is observed at -800 ppm. The intensity of the main peak increases with the delay time and saturates at 2500 ms. The main peak of ^{125}Te NMR for Bi_2Te_3 (#2) is observed at -180 ppm; a moderate shoulder is observed at -660 ppm. The peak position is determined not only by the chemical shift due to effects from local environment, but also by the Knight shifts due to effects from free charge carrier concentration).[25,26] In Bi_2Te_3 samples #1 and #2, different peak position is mostly due to the Knight shift, which agrees well with different free (mobile) carrier concentrations; this is supported by the Hall effect measurements (Table 2). The intensity of the peak also increases with the delay time and saturates at 600 ms, i.e. much faster than Bi_2Te_3 (#1). Small distortion of NMR spectra observed at the left of the main peak for short delay times shows a contribution from some Te in Bi_2Te_3 (#2).

^{125}Te NMR spectra of both our Bi_2Te_3 samples shown on Figs. 3a,b demonstrate the presence of Te atoms in different environments: the main peak from Te atoms surrounded mostly

by Bi and the right shoulder from Te close to antisite defects. The ratio of intensities of the main peak and defect sites is ~16 for sample #1 and ~6 for sample #2. The ratio between these values is ~2.6, which is close to the ratio of the carrier concentration in samples #2 and #1, ~2.5, i.e., the right shoulders reflect the carrier concentration produced by antisite defects.

Figures 4a and 4b show ^{125}Te NMR spectra for both Bi_2Te_3 samples with the signal intensities rescaled to the value obtained for the saturated spectra. The spectra for Bi_2Te_3 (#1) do not change, in general, their shape and frequencies, i.e. there is no significant amount of Te which can produce a signal at higher and particularly at lower frequencies. In contrast, the spectra for Bi_2Te_3 (#2) shows some contribution to the signal at both the lower and higher frequencies, forming the left and right shoulders. The right shoulder is similar to that observed for Bi_2Te_3 (#1), but has larger intensity, whereas the left shoulder was not observed for Bi_2Te_3 (#1) (Fig. 3).

The resonance frequency, i.e. the total shift of NMR signal position, δ_{total} , relative to a reference, is the sum of the chemical shift, δ_{chem}, due to chemical environment, and the Knight shift, K, due to a hyperfine interaction between nuclei and free charge carriers.[25,26] The different signal resonance frequencies observed for Bi_2Te_3 samples #1 and #2 suggest different chemical and/or Knight shifts, which, in principle, can be tested by spin-lattice relaxation measurements. Note that nuclei relaxation in metals and semiconductors is mostly determined by the hyperfine interaction of nuclei with free charge carriers [26] and affect the signal position via the Knight shift, which depends on T_1 via the Korringa relation $K^2T_1T = const$, T is the absolute temperature, or $K^2T_1 = const$ at a given temperature.[27] In complex tellurides the Korringa relation at a given temperature can be used for estimation of possible Knight shift vs. measured T_1.

When spin-lattice relaxation contains one component, fitting of the dependence of the normalized peak intensity on the saturation recovery time can be conducted by the equation [7,18]

$$I(t) = 1 - e^{-t/T_1} \quad (1)$$

However, multicomponent tellurides typically are chemically and electronically inhomogeneous and spin-lattice relaxation may contain at least two components and normalized peak intensity vs. saturation recovery time requires a bi-exponential fit

$$I(t) = f_A(1 - e^{-t/T_{1,A}}) + f_B(1 - e^{-t/T_{1,B}}) \quad (2)$$

where f_A and f_B are fractions of components *A* and *B* in the material, and $T_{1,A}$ and $T_{1,B}$ are the spin-lattice relaxation times of these components. [7,18]

In addition, relaxation processes can be described by the stretched exponential relaxation function.[10,20,28] This function can be used to describe ^{125}Te NMR spin-lattice relaxation tellurides via the equation

$$I(t) = I_0\left(1 - \exp\left(\frac{t}{T_1}\right)^{\beta}\right) \quad (3)$$

where β is the Kohlrausch exponent; this equation was used to fit ^{125}Te NMR for Bi_2Te_3 and related materials.[10,20] We test all three equations to describe ^{125}Te NMR spin-lattice relaxation in our Bi_2Te_3 samples.

Figure 5a shows normalized intensity of ^{125}Te NMR signal vs. saturated recovery time (delay time) for the peak for Bi_2Te_3 (#1); the value of T_1 for the main signal (peak) obtained from the plots is 300 ms. However, the peak for Bi_2Te_3 (#1) can be fit by two components (Eq. 2), short relaxation component with $T_{1,A}$ = 100 ms and long component with $T_{1,B}$ = 700 ms, of the same fractions, 0.5. The inset in Fig. 5a shows dependence of 1-*I*, where *I* is the intensity of ^{125}Te NMR signal, vs. saturation recovery time (delay time) and also demonstrates the existence

of two relaxation components. The intensities of the right shoulder for Bi_2Te_3 (#1) as well as the left shoulder for Bi_2Te_3 (#2) are too small to perform a reliable quantitative analysis of its changes with delay time, but it is clear that they can be attributed to Te in the environment with T_1 longer and shorter, respectively, compared to that of the main peak.

Figure 5b shows normalized intensity of ^{125}Te NMR signal vs. saturated recovery time (delay time) for the peak for Bi_2Te_3 (#2); the value of T_1 for the main signal (peak) and the shoulder obtained from the plots are 70 and 300 ms. The peak can be fit also by one component (Eq. 1) with T_1 = 70 ms whereas the shoulder can be fit by two components (Eq. 2), a short component with $T_{1,A}$ = 100 ms and long component with $T_{1,B}$ = 800 ms, of the same fractions, 0.5. The inset in Fig. 5b shows dependence of 1-I for the peak and shoulder and confirms one component for the peak and two components for the shoulder. The peak for Bi_2Te_3 (#2) also can be fit by Eq. 3 with T_1 = 70 ms and $\beta = 1$, i.e., it can also be fit by Eq. 1. Note that Eq. 3 cannot provide good fit for the main peak for Bi_2Te_3 (#1) and for the right shoulder for Bi_2Te_3 (#2), which limits its application to our Bi_2Te_3 samples.

Earlier, it was shown that the carrier concentration in GeTe-based materials can be obtained using known carrier concentration and T_1 values in GeTe.[7,8] Both our Bi_2Te_3 samples (and likely all Bi_2Te_3 samples [3,11]) show multicomponent spin-lattice relaxation due to atomic defects, which generate free charge carriers and form electronically inhomogeneous systems. It is important to understand how the values of the carrier concentrations derived from ^{125}Te NMR spin-lattice relaxation measurements in electronically inhomogeneous materials (differential parameters) are relevant to the value obtained from the Hall effect (integral parameter), and how these values are relevant to the Seebeck coefficient (integral parameter).

To calculate the carrier concentration in Bi_2Te_3 samples, a reference electronically homogeneous material with known carrier concentration and T_1 is needed. If GeTe is used as a reference, the carrier concentration in both Bi_2Te_3 samples obtained using Maxwell-Boltzmann ($1/T_1 \sim n$) or Fermi-Dirac ($1/T_1 \sim n^{2/3}$) statistics [8,25,26] for all T_1 values obtained from experiment by fitting (Table 2) is, in general, much lower than that obtained from the Hall effect; this means that GeTe cannot be used as reference.

On the other hand, we can estimate the value of T_1, which can be attributed to the carrier concentration obtained from the Hall effect using ratios between the Seebeck coefficients, carrier concentrations, and T_1. The ratios between the Seebeck coefficients and free carrier concentrations in Bi_2Te_3 (#1) and Bi_2Te_3 (#2) samples can be written as $S_{\#1}/S_{\#2} = \left(n_{\#2}/n_{\#1}\right)^{2/3}$, where $S_{\#1}$ and $n_{\#1}$, $S_{\#2}$ and $n_{\#2}$ are the Seebeck coefficients and carrier concentrations of Bi_2Te_3 (#1) and Bi_2Te_3 (#2) samples, respectively. Using Maxwell-Boltzmann statistics for the analysis of the Seebeck coefficient via NMR data, this ratio can be written as $S_{\#1}/S_{\#2} = \left(T_{1,\#2}/T_{1,\#1}\right)^{2/3}$. The challenge is what T_1 values should be used in this estimation.

It is clear that separate $T_{1,A}$ and $T_{1,B}$ values for both samples cannot be used in calculations, and the challenge is if the average T_1 value calculated for each sample will be acceptable. The average values of spin-lattice relaxation time, $T_{1,av}$, can be calculated separately for the main peak and the right shoulder as $T_{1,av} = (T_{1,A})(f_A)+(T_{1,B})(f_B)$ (see Table 2). For Bi_2Te_3 (#1), spin-lattice relaxation time, $T_{1,\#1}$, calculated based on only the data for the main peak (the right shoulder is too small to be analyzed), will be the same as $T_{1,av}$, i. e. $T_{1,\#1}$ = 400 ms. For Bi_2Te_3 (#2), $T_{1,\#2}$ should be calculated using spin-lattice relaxation time values for both the main peak, 70 ms, and $T_{1,av}$ for the shoulder, 450 ms (Table 2).

Based on the intensities of the main peak and shoulder for Bi_2Te_3 (#2) (72 and 28%, respectively), $T_{1,\#2}$ = 176 ms. Hence, $\left(T_{1,\#1} / T_{1,\#2}\right)^{2/3}$ = (400 ms/176 ms)$^{2/3}$ = 1.73, which is just slightly smaller than $S_{\#1} / S_{\#2}$ = 1.88 (see above) and $\left(n_{\#2} / n_{\#1}\right)^{2/3}$ = 1.84. If Fermi-Dirac statistics is used for calculations, $T_{1,\#1} / T_{1,\#2}$ = 400 ms/176 ms = 2.27, which is larger compared to the value obtained using Maxwell-Boltzmann statistics. Both statistics show that the average values of spin-lattice relaxation times can, in general, be used for estimation of the free carrier concentrations in electronically inhomogeneous materials, but Maxwell-Boltzmann statistics provide a better fit with experimental values of the Seebeck coefficients and carrier concentration obtained from the Hall effect.

It also is clear that electronic inhomogeneity in complex tellurides can affect electronic and thermal transport, but the number of experimental methods, which can detect such inhomogeneity, is quite limited. For example, microscale Seebeck coefficient scanning demonstrates dramatic changes in the value and even in sign of the Seebeck coefficient of PbTe alloyed with Ag and Sb.[29] Because XRD of these materials shows a single phase, such changes were explained by slight local variations in composition. Note that PbTe and GeTe represent self-doping semiconductors, where the charge carrier concentration can be changed by the Pb/Te and Ge/Te ratio, and in addition the replacement of Ge in GeTe by Ag or Sb can decrease or increase the carrier concentration and result in electronic inhomogeneity in the case of Sb. [8]

Electronic inhomogeneity in PbTe- and GeTe-based materials at the atomic level also was detected by ^{207}Pb and ^{125}Te NMR. [5,8,18] ^{125}Te NMR shows that even *p*- and *n*-types PbTe samples are electronically inhomogeneous, which reflects that the Pb/Te ratio even in PbTe is nonuniform. [18] In this study, the ^{125}Te NMR spectra and spin-lattice relaxation measurements also demonstrate that both Bi_2Te_3 samples are electronically inhomogeneous at the atomic scale,

which can be attributed to a different Te environment due to spatial variation of the Bi/Te ratio resulting in various atomic defects. In general, in Bi-rich Bi_2Te_3 sample, Bi_{Te} and/or V_{Te} defects, whereas in Te-rich Bi_2Te_3 sample, Te_{Bi} and V_{Bi} defects are expected to be formed. [20,21] Hence, ^{125}Te NMR signals observed for different Bi_2Te_3 single-phase samples can be produced by $Te_{(1)}$ and $Te_{(2)}$ atoms, as well as by Te close to the atomic defects, which may change their environment.

The sum of $Te_{(1)}$ and $Te_{(2)}$ atoms in Bi_2Te_3 (#1) and (#2) samples would be similar, and ^{125}Te NMR main peaks in both samples can be attributed to all these Te atoms. Bi_2Te_3 (#1) shows *p*-type conductivity, which can be explained by the presence of mostly Bi antisite defects, Bi_{Te}, and in addition possibly by Bi vacancy defects, V_{Bi}. Note that Bi_{Te} defects in Bi_2Te_3 synthesized from the stoichiometric melt are preferred, [3,20] and the right shoulder of small intensity in *p*-type Bi_2Te_3 (#1) should be attributed to Te atoms, which are close to Bi_{Te} antisite defects. The hole concentration in Bi_2Te_3 (#1) obtained from the Hall effect is relatively low (Table 2), which agrees well with a large Seebeck coefficient (Fig. 2), and can be used as evidence for the presence of Bi_{Te} antisite defects of low concentration.

Bi_2Te_3 (#2) shows *n*-type conductivity, which can be explained by the presence of Te antisite defects, Te_{Bi}; the contribution from Te vacancy defects, V_{Te}, is unlikely. Note that Te_{Bi} defects in Bi_2Te_3 synthesized from the Te-rich melt are preferred, [20,21] and the right shoulder in *n*-type Bi_2Te_3 (#2) can be attributed to Te atoms, which are close to Te_{Bi} antisite defects. The larger intensity of the shoulder in Bi_2Te_3 (#2) compared to that in Bi_2Te_3 (#1) can be explained by the higher concentration of Te_{Bi}. This agrees well with the higher carrier concentration obtained from the Hall effect (Table 2) and smaller absolute value of the Seebeck coefficient (Fig. 2) at 300 K.

Using our room temperature Seebeck coefficients and that reported by Satterthwaite and Ure,[30] we can suggest a likely composition of Bi_2Te_3 samples #1 and #2. For our *n*-type Bi_2Te_3 (#2), S = -130 μV K^{-1} can be attributed to ~63 at.% Te in melt. For *p*-type Bi_2Te_3 (#1), S =+250 μV K^{-1} is larger by ~20% compared to that for Bi_2Te_3 containing less than 62 at.% Te in melt. One of the reasons of such discrepancies can be different methods of the Seebeck coefficient measurements in Ref. 30 and used by us. Note also that if the amount of Te in Bi_2Te_3 is estimated based on the carrier concentration using our values from Table 1 and the data from Ref. 30, Bi_2Te_3 sample #2 may contain ~66 at.% Te, whereas #1 contains ~61 at.% Te.

^{125}Te NMR signal for Bi_2Te_3 (#2) with relatively short T_1 observed at the left of the main peak (Fig. 4b) should be attributed to Te located in the area with relatively high free carrier concentration. We suggest that the higher carrier concentration can be attributed to small amount of Te atoms close to V_{Bi}; electron configurations of Bi ($6p^3$) and Te ($5p^2$) show that each Bi vacancy can generate three holes, whereas Bi_{Te} and Te_{Bi} antisite defects generate one hole and one electron, respectively.

Because dominant free charge carriers in Bi_2Te_3 (#2) are electrons, the holes generated by V_{Bi} are compensated by electrons generated by Te_{Bi} antisite defects. The NMR signal at the left of the main peak in Bi_2Te_3 (#1) is not detected because it is unlikely that V_{Bi} in this sample can be formed. It should also be noted here that the resonance frequency of all ^{125}Te NMR signals, observed for our Bi_2Te_3 samples and its dependence on delay time are determined by the interplay between the chemical and Knight shifts and can be assigned to Te in environments with different local composition and free carrier concentration formed by atomic defects.

4. SUMMARY

Two single crystalline samples of Bi_2Te_3 grown (i) using Bridgman technique, sample Bi_2Te_3 (#1), and (ii) out of Te-rich high temperature flux, Bi_2Te_3 (#2), have been studied. XRD patterns show that both samples are single-phase. At 300 K, the value of the Seebeck coefficient of Bi_2Te_3 (#1) is positive, +250 μV K^{-1} (*p*-type), whereas that of Bi_2Te_3 (#2) is negative, -133 μV K^{-1} (*n*-type), and agrees well with the Hall effect data showing lower hole concentration and higher electron concentration, respectively. ^{125}Te NMR for both samples show a peak and shoulder, which reflect the presence of Te in different environments. ^{125}Te NMR spin-lattice relaxation measurements show that the peak in Bi_2Te_3 (#1) can be fit by two components spin-lattice relaxation time, $T_{1,A}$ and $T_{1,B}$. The intensity of the shoulder in Bi_2Te_3 (#1) is too small to be fit. The peak observed for Bi_2Te_3 (#2) can fit by one T_1 component, whereas the shoulder can be fit by two components; this means both materials are electronically inhomogeneous. ^{125}Te NMR peaks observed for both Bi_2Te_3 (#1) and Bi_2Te_3 (#2) can be attributed to the majority of Te atoms surrounded by Bi, whereas the shoulders to Te atoms close to Bi_{Te} or Te_{Bi} antisite defects, respectively. ^{125}Te NMR spectroscopy and spin-lattice relaxation measurements is an effective probe to study antisite defects in Bi_2Te_3 and related tellurides, and along with the Seebeck coefficient measurements enable better understanding of their effect on electronic transport.

AUTHOR INFORMATION
Corresponding Author
E-mail levin@iastate.edu, Tel: 1-515-294-6093 (E.M.L.)

Notes
The authors declare no competing financial interest

ACKNOWLEDGEMENTS

Authors thank the Materials Preparation Center at the Ames Laboratory U.S. Department of Energy (DOE) for sample synthesis. This work was supported by the U.S. Department of Energy, Office of Basic Energy Sciences, Division of Materials Sciences and Engineering. The research was performed at the Ames Laboratory, which is operated for the U.S. Department of Energy by Iowa State University under Contract No DE-AC02-07CH11358.

REFERENCES

(1) Goldsmid, H. J. *Thermoelectric refrigeration*. Springer, Science + Business Media, New York, **1964**.

(2) Hasan M. Z.; Kane, C. L. Topological insulators. *Rev. Mod. Phys*. **2010**, *82*, 3045-3067.

(3) Scanlon, D. O.; King, P. D. C.; Singh, R. P.; De la Torre, A.; McKeown Walker, S.; Balakrishnan, G.; Baumberger, F.; Catlow, C. R. A. Controlling bulk conductivity in topological insulators: key role of anti-site defects. *Adv. Mater*. **2012**, *24*, 2154-2158.

(4) Alexander, M. N.; Sagalyn, P. L.; Senturia, S. D.; Hewes, C. R. Nuclear spin relaxation study of the electronic structure of lead telluride. *J. Nonmetals* **1973**, *1*, 251-256.

(5) Levin, E. M.; Cook, B. A.; Ahn, K.; Kanatzidis, M. G.; Schmidt-Rohr, K. Electronic inhomogeneity and Ag:Sb imbalance of $Ag_{1-y}Pb_{18}Sb_{1+z}Te_{20}$ high-performance thermoelectrics elucidated by ^{125}Te and ^{207}Pb NMR. *Phys. Rev. B* **2009**, *80*, 115211.

(6) Levin, E. M.; Besser, M. F.; Hanus, R. Electronic and thermal transport in GeTe: a versatile base for thermoelectric materials. *J. Appl. Phys*. **2013**, *114*, 083713.

(7) Levin, E. M.; Hanus, R.; Hanson, M.; Strazsheim, W.; Schmidt-Rohr, K. Thermoelectric properties of $Ag_2Sb_2Ge_{46-x}Dy_xTe_{50}$ alloys with high power factor. *Physica Status Solidi A* **2013**, *210*, 2628-2637.

(8) Levin, E. M. Effect of Ge substitution in GeTe by Ag or Sb on the Seebeck coefficient and carrier concentration derived from ^{125}Te NMR. *Phys Rev B* **2016**, *93*, 045209.

(9) Taylor, R. E.; Leung, B.; Lake, M. P.; Bouchard, L.-S. Spin-lattice relaxation in bismuth chalcogenides. *J. Phys. Chem. C* **2012**, *116*, 17300-17305.

(10) Koumoulis, D.; Chasapis, T. C.; Taylor, R. E.; Lake, M. P.; King, D.; Jarenwattananon, N. N.; Fiete, G. A.; Kanatzidis, M. G.; Bouchard, L.-S. NMR probe of metallic states in nanoscale topological insulators. *Phys. Rev. Lett*. **2013**, *110*, 026602.

(11) Fleurial, J. P.; Gailliard, L.; Triboulet, R.; Scherrer H.; Scherrer, S. Thermal properties of high quality single crystals of bismuth telluride-part I: experimental characterization. *J. Phys. Chem. Solid* **1988**, *49*, 1237-1247.

(12) Canfield, P. C.; Kong, T.; Kaluarachi, U. S.; Jo, N. H. Use of frit-disc crucible for routine and exploratory solution growth of single crystalline samples. *Philos. Mag. B* **2016**, *96*, 84-92.

(13) Canfield, P. C.; Fisk, Z. Growth of single crystals from metallic fluxes. *Philos. Mag. B* **1992**, *65*, 1117-1123.

(14) ASM Alloy Phase Diagram Database: www1.asminternational.org/ (accessed June 10, 2016).

(15) Wang, G.; Endicott, L.; Uher, C. In *Thermoelectric Bi_2Te_3 Nanomaterials*. Willey-VCH, Ed. by Eible, O.; Nielsch, K.; Peranio, N.; Volklein, F. Weinheim, Germany, **2015**. Ch. 5, p. 73-98.

(16) Nakajima, S. J. The crystal structure of $Bi_2Te_{3-x}Se_x$. *J. Phys. Chem. Solids* **1963**, 24, 479-485.

(17) Yavorsky, B. Yu.; Hinsche, N. F.; Mertig, I.; Zahn, P. Electronic structure and transport anisotropy of Bi_2Te_3 and Sb_2Te_3. *Phys. Rev. B* **2011**, *84*, 165208.

(18) Levin, E. M.; Heremans, J. P.; Kanatzidis, M. G.; Schmidt-Rohr, K. Electronic inhomogeneity in *n*- and *p*-type PbTe detected by ^{125}Te NMR. *Phys. Rev. B* **2013,** *88*, 115211.

(19) Miller, G. R.; Li, C. Y. Evidence for the existence of antistructural defects in bismuth tellurides by density measurements. *J. Phys. Chem. Solids* **1965**, *26*, 173-177.

(20) Koumoulis, D.; Leung, B.; Chasapis, T. C.; Taylor, R.; King, D. Jr; Kanatzidis, M. G.; Bouchard, L.-S. Understanding bulk defects in topological insulators from nuclear-spin interactions. *Adv. Funct. Mater*. **2014**, *24*, 1519-1528.

(21) A. Hashibon, A.; Elsasser, C. In *Thermoelectric Bi_2Te_3 Nanomaterials*. Willey-VCH, Ed. by O. Eible, K. Nielsch, N. Peranio, and F. Volklein. Weinheim, Germany, 2015. Ch. 9, p. 167-186.

(22) Oh, M. W.; Son, J. H.; Kim, B. S.; Park, S. D.; Min, B. K.; Lee, H. W. Antisite defects in n-type $Bi_2(Te,Se)_3$: experimental and theoretical studies. *J. Appl. Phys*. **2014**, *115*, 133706.

(23) Hashibon, A.; Elsasser, C. First-principle density functional theory study of native point defects in Bi_2Te_3. *Phys. Rev. B* **2011**, *84*, 144117.

(24) Snyder, G. J.; Toberer, E. S. Complex thermoelectric materials. *Nature Mater*. **2008**, 7, 105-114.

(25) Selbach, H.; Kanert, O.; Wolf, D. NMR investigation of the diffusion and conduction properties of the semiconductor tellurium. I. Electronic properties. *Phys. Rev. B* **1979**, *19*, 4435-4443.

(26) Yesinowski, J. P. Solid-state NMR of inorganic semiconductors. *Top. Curr. Chem*. **2012**, *306*, 229-312.

(27) Yesinowski, J. P.; Purdy, A. P.; Wu, H.; Spencer, M. G.; Hunting, J.; DiSalvo, F. J. Distribution of conduction electrons as manifested in MAS NMR of gallium Nitride. *J. Am. Chem. Soc*. **2006**, *128*, 4952-4953.

(28) Johnston, D. C. Stretched exponential relaxation arising from a continuous sum of exponential decays. *Phys. Rev. B* **2006**, *74*, 184430.

(29) Chen, N.; Gascoin, F. G.; Snyder, G. J.; Muller, E.; Karpinski, G.; Stiewe, C. Macroscopic thermoelectric inhomogeneities in $(AgSbTe_2)_x(PbTe)_{1-x}$. *Appl. Phys. Lett*. **2005**, *87*, 171903.

(30) Satterthwaiste, C. B; Ure, Jr., R. W. Electrical and thermal properties of Bi_2Te_3. *Phys. Rev.* **1957**, *108*, 1164-1170.

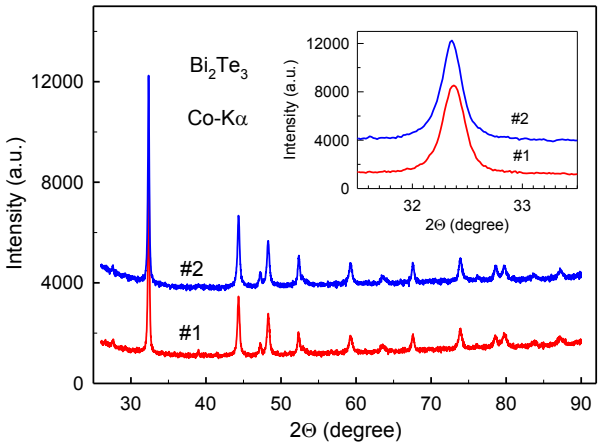

Figure 1. XRD (Co-K_α, $\lambda = 0.1789$ nm) patterns of Bi_2Te_3 samples #1 and #2 at 300 K. The inset shows an expanded view for the main peak at $31.5° \leq 2\Theta \leq 33.5°$.

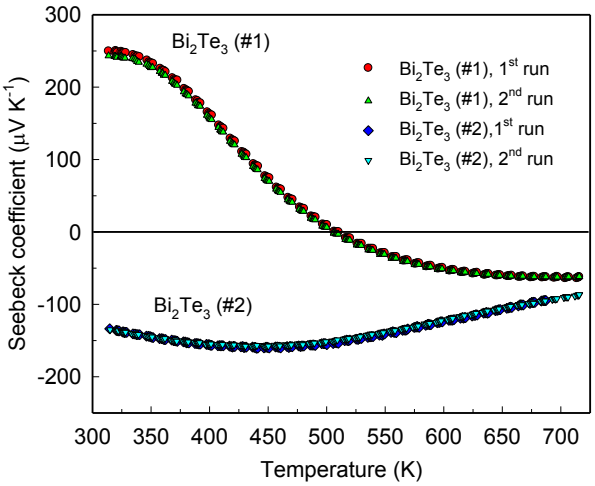

Figure 2. Temperature dependencies of the absolute Seebeck coefficient of Bi_2Te_3 samples #1 and #2, showing stability of the Seebeck coefficient and different type of conductivity at 300 K.

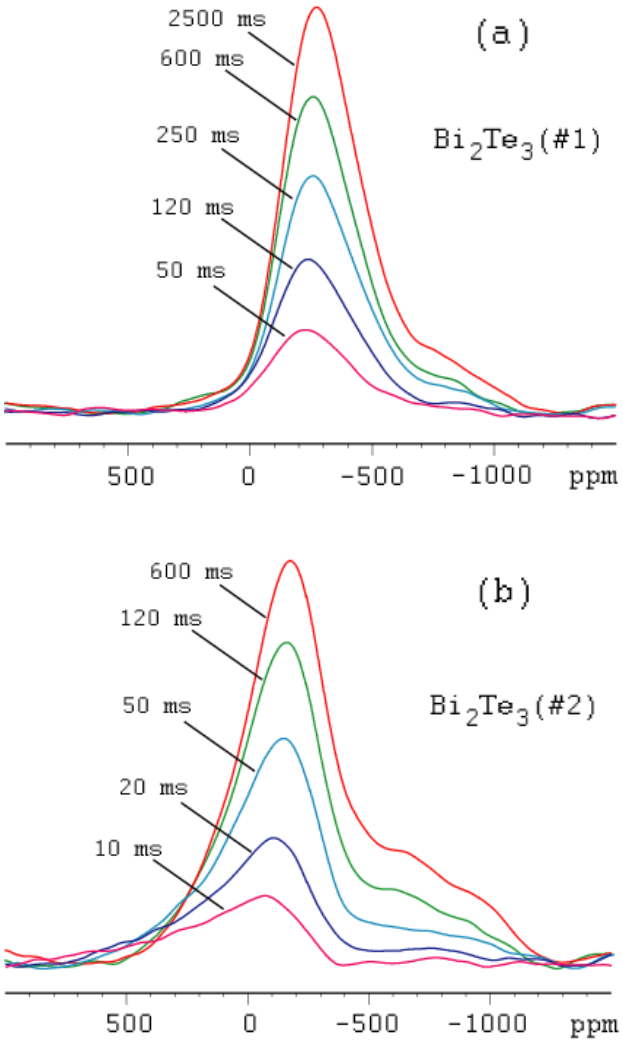

Figure 3. ^{125}Te NMR spectra of Bi_2Te_3 samples (a) #1 and (b) #2 obtained at 300 K for various saturation recovery (delay) times.

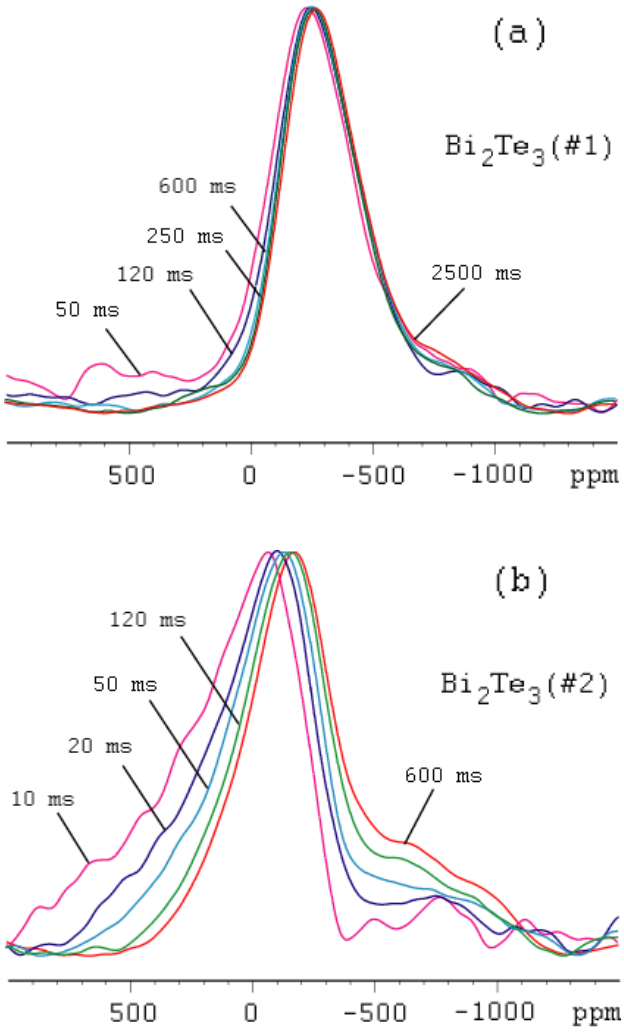

Figure 4. ^{125}Te NMR spectra of Bi_2Te_3 samples (a) #1 and (b) #2 obtained at 300 K for various saturation recovery (delay) times and rescaled to the value obtained for the saturated spectra.

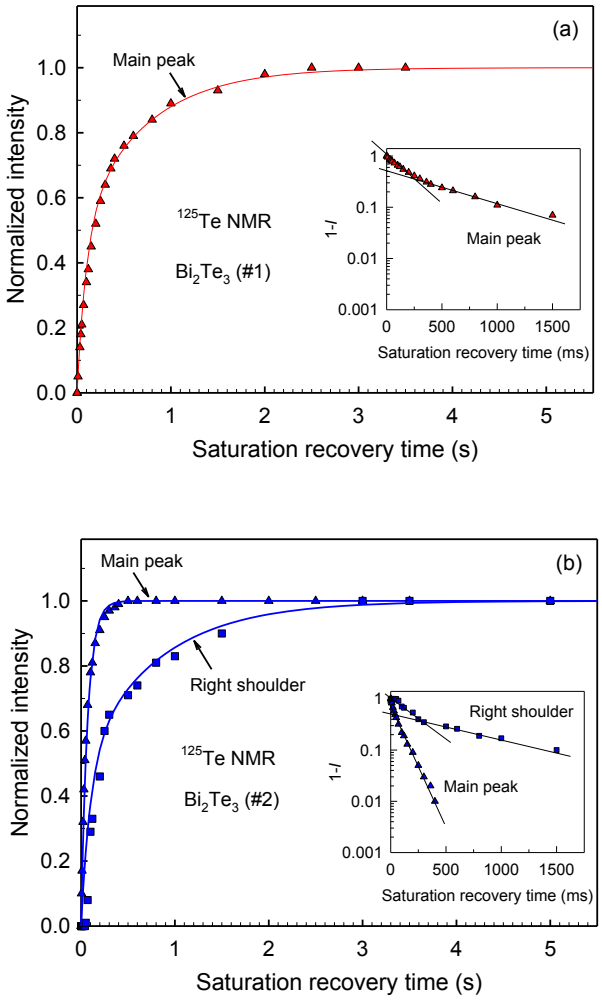

Figure 5. ^{125}Te NMR spin-lattice relaxation for Bi_2Te_3 samples (a) #1 and (b) #2 at 300 K. The insets in (a) and (b) show semilogarithmic plots of (1-*I*) vs saturation recovery time, which can be fit by two spin-lattice relaxation times, $T_{1,A}$ and $T_{1,B}$, for the main peak in (a) and for the right shoulder in (b), and by one T_1 component for the main peak in (b). The right shoulder for Bi_2Te_3 (#1) (Fig. 3a) and the left shoulder for Bi_2Te_3 (#2) (Fig. 4b) are too small for analysis.

Table 1

Lattice parameters of Bi_2Te_3 samples at 300 K calculated for hexagonal and rhombohedral structures.

Sample	Hexagonal structure		Rhombohedral structure	
	a (Å)	c (Å)	$a = b =$ c (Å)	$\alpha = \beta = \gamma$ (°)
Bi_2Te_3 (#1)	4.386	30.509	10.480	24.16
Bi_2Te_3 (#2)	4.385	30.478	10.470	24.18
Bi_2Te_3	4.386[a]	30.497[a]	10.473[b]	24.17[b]

a - Ref. 16
b - Ref. 17

Table 2

^{125}Te NMR main peak and right shoulder positions, spin-lattice relaxation time, T_1, Seebeck coefficient, and carrier concentration obtained from the Hall effect for Bi_2Te_3 samples at 300 K.

Sample	^{125}Te NMR signal position (ppm)		Spin-lattice relaxation time, T_1		Seebeck coefficient (μV K^{-1})	Carrier concentration from Hall effect ($\times 10^{19}$ cm^{-3})
	Peak	Right shoulder	Peak	Right shoulder		
Bi_2Te_3 (#1)	-270	-800	$T_{1,A}$=100 ms, f_A=0.5 $T_{1,B}$=700 ms, f_B=0.5 $T_{1,av}$=400 ms	Too small intensity	+250	1.2 (*p*-type)
Bi_2Te_3 (#2)	-180	-660	T_1=70 ms	$T_{1,A}$=100 ms, f_A=0.5 $T_{1,B}$=800 ms, f_B=0.5 $T_{1,av}$=450 ms	-133	3.0 (*n*-type)